Fragile-to-strong crossover, growing length scales, and dynamic heterogeneity in Wigner glasses

Hyun Woo Cho, Mauro L. Mugnai, T. R. Kirkpatrick, and D. Thirumalai

Phys. Rev. E **101**, 032605 — Published 17 March 2020

DOI: 10.1103/PhysRevE.101.032605

Fragile-to-Strong Crossover, growing length scales, and dynamic heterogeneity in Wigner Glasses

Hyun Woo Cho[1], Mauro L. Mugnai[1], T. R. Kirkpatrick[2] and D. Thirumalai[1]
[1] *Department of Chemistry, University of Texas at Austin, Austin, Texas 78712, USA and*
[2] *Institute for Physical Science and Technology, University of Maryland, College Park, Maryland 20742, USA*
(Dated: February 25, 2020)

Colloidal particles, which are ubiquitous, have become ideal testing grounds for the structural glass transition (SGT) theories. In these systems glassy behavior arises as the density of the particles is increased. Thus, soft colloidal particles with varying degree of softness capture diverse glass forming properties, observed normally in molecular glasses. Brownian dynamics simulations for a binary mixture of micron-sized charged colloidal suspensions show that tuning the softness of the interaction potential, achievable by changing the monovalent salt concentration results in a continuous transition from fragile to strong behavior. Remarkably, this is found in a system where the well characterized interaction potential between the colloidal particles is isotropic. We also show that the predictions of the random first order transition (RFOT) theory quantitatively describes the universal features such as the growing correlation length, $\xi \sim \left(\frac{\phi_K}{\phi} - 1\right)^{-\nu}$ with $\nu = \frac{2}{3}$ where ϕ_K, the analogue of the Kauzmann temperature, depends on the salt concentration. As anticipated by the RFOT predictions, we establish a causal relationship between the growing correlation length and a steep increase in the relaxation time and dynamic heterogeneity as the system is compressed. The broad range of fragility observed in Wigner glasses is used to draw analogies with molecular and polymer glasses. The large variations in the fragility are normally found only when the temperature dependence of the viscosity is examined for a large class of diverse glass forming materials. In sharp contrast, this is vividly illustrated in a single system that can be experimentally probed. Our work also shows that the RFOT predictions are accurate in describing the dynamics over the entire density range, regardless of the fragility of the glasses.

INTRODUCTION

The abiding interest in the structural glass transition (SGT) problem, which occurs readily in a large class of materials either by supercooling or by compression, is a testimony to its importance in condensed matter physics. Extensive experimental, theoretical, and computer simulation studies have established that the Random First Order Transition (RFOT) theory [1] provides a reasonable description of many important characteristics of the SGT. Several reviews [2–7] have discussed the theoretical underpinnings and applications of the RFOT theory to not only to SGT but a number of other fields [7]. Although the RFOT theory was inspired by a class of precisely soluble mean field spin glass models lacking inversion symmetry in the presence of quenched randomness [8–12], it was shown that the major results could also be derived using a density functional Hamiltonian for liquids where the randomness is self-generated [13], just as in the SGT (see also [14, 15]). Because the theoretical approaches were inherently mean field-like, which although one could argue is accurate in liquids, additional studies were needed to assess the robustness of the RFOT conclusions. There are connections between equilibrium and dynamical transitions in large dimensions [16], which are explicit in spin glass models without inversion symmetry. These have made precise in a number of remarkable studies [17–19], which established that RFOT is exact in $d = \infty$ dimensions for hard sphere glass forming systems. These studies provide support to the original suggestion [1, 13] that the physics underlying RFOT describes the SGT problem fairly accurately.

A prediction of the RFOT is that for a generic glass forming system there are two major transitions as the liquid is compressed (increase in the volume fraction of the particles, ϕ). We focus on ϕ, and not the temperature because that is the the relevant variable in the binary mixture of charged colloidal suspensions, which undergo a liquid to glass (Wigner glass) transition at high enough values of ϕ [20]. At a $\phi \sim \phi_d$ there is a dynamical transition at which the transport starts to become sluggish although signatures of slow dynamics is evident even at values of ϕ less than ϕ_d. As the liquid is compressed further (ϕ is increased) there is an ideal glass transition at ϕ_K (analogue of the Kauzmann temperature) at which the configurational entropy vanishes, which in turn results in complete cessation of motion. If undercooled by lowering the temperature instead of increasing ϕ, the ideal glass transition occurs at T_K where there is an essential singularity in the temperature dependence of the viscosity. Of course, the transition at ϕ_d and the thermodynamic transition at ϕ_K are connected, which is needed to provide a consistent picture of the SGT [2, 7]. The topology of the state space is unremarkable at $\phi < \phi_d$ where collective transport is not prominent. On the other hand, for $\phi > \phi_d$ the dynamics slows down because the system is trapped in one of the exponentially large number of metastable states [13]. Under these circumstances transport becomes possible only by overcoming free en-

ergy barriers separating the metastable states. The time scales for crossing the barriers can be arbitrarily long depending on ϕ, and becomes essentially infinite at ϕ_K. The two transition picture and the associated scaling relations of quantities, such as the growing length scales and the surface tension between two mosaic states at values of $\phi > \phi_d$ (or $T < T_d$), approaching the ideal glass transition volume fraction ϕ_K (or T_K), have been measured both in computer simulations using predominantly hard spheres (HS) or Lennard-Jones (LJ) or soft sphere (SS) mixtures [21–27] and experiments [28–31].

One of the hallmarks of glass forming materials is that they exhibit dramatically different curvatures when $\log \eta$ is plotted as a function of $\frac{T_g}{T}$ where η is the shear viscosity, T_g is the glass transition temperature, which is operationally defined using $\eta(T_g) \simeq 10^{13}$ poise or when the structural relaxation time reaches about 100 seconds. In the graph of $\log \eta$ as a function of $\frac{T_g}{T}$, often referred to as the Angell plot [32], classic glass formers, such as *ortho*-terphenyl or Trehalose are "fragile" as are mixtures of HS, LJ or SS particles. In contrast, Si or SiO_2, which are network forming materials with anisotropic interaction potentials, are classified as "strong" glasses. In fragile glasses, the effective activation free energies separating the metastable states explored above ϕ_d increase sharply as the system is continuously compressed whereas they are relatively independent of ϕ in strong glasses. Fragile and strong glasses are often discussed in terms of the fragility index [33].

Here, we have two goals in mind. First, we demonstrate using mixtures of glass forming highly charged micron-sized colloidal suspensions (classical Wigner glasses) that the key predictions of RFOT are quantitatively validated, adding to the growing evidence that RFOT theory seamlessly explains the dynamics **both** below ϕ_d and also in the density range spanning $\phi_d \leq \phi \leq \phi_K$. Second, we show that there is a crossover from fragile to strong behavior in Wigner glasses as the concentration of monovalent salt is increased. The large change in the fragility index needed for the crossover occurs in just one system even though the interparticle potential is isotropic. These new predictions can be tested using optical microscopy techniques [30].

The key to our findings is the recognition that stiffness of the interparticle potentials in colloids can be changed by controlling the surface charge or internal elasticity of colloids [34]. Examples of such systems include emulsions [28], microgels [35–37], charged colloids [37], and squishable cells [38, 39]. These systems display glass-like properties that are distinct compared to fragile hard-sphere like systems. Most striking impact of the softness on the glass transition is that "fragility" of colloids can be greatly modified upon change in the stiffness of the potential, which in turn can be altered by changing the interaction potentials [35]. For the much less investigated Wigner glasses, the fragility is a measure of how steeply the relaxation time τ_α increases near the glass transition volume fraction ϕ_g. Since the first experiments using microgels as soft glasses [35], several studies revealed that the glass transition of soft colloids can be either strong or fragile depending on the stiffness [40–43]. Upon decreasing the stiffness of the interaction potential between the colloids the fragility increases. Thus, soft colloids can be exploited as important model systems that mimic the characteristics of diverse glass forming materials [44].

Despite several examples, the physics underlying the fragile-to-strong crossover in soft colloids is not fully understood. First, whether the softness does really contribute to the drastic change in the fragility remains controversial. Indeed, in several experiments [36, 37, 45, 46], it was found that the fragility in soft colloids is insensitive to the softness of the interaction potentials. Previous simulations with model soft colloids showed that the drastic variation in the fragility cannot be reproduced by merely modifying the softness of the potential [37, 47–49]. Thus, some have argued that the softness does not dominate the fragility of colloidal glasses. Instead, it was suggested that other mechanisms relying on the the microscopic details of the soft colloids are important for the drastic change in the fragility in the previous experiments [37, 50–52]. Here, we elucidate the effect of the softness on the fragility of soft colloids in order to resolve the conflicting interpretations.

Second, as a simplest realization of the diverse glass forming liquids, whether the glass transition in soft colloids with a broad spectrum of the fragility can be described universally is a question of fundamental importance. The sluggish dynamics near the glass transition is attributed to the sudden increase in the effective free energy barriers controlling structural relaxation at $\phi > \phi_d$. Thus, the fragility of liquids depends on how steeply the effective free energy barrier increases near the glass transition. As alluded to above, the RFOT theory naturally explains the increase in the free energy barrier near the glass transition, which is due to the emergence of a growing length scale in which dynamics of the particles are highly correlated [1, 7, 53]. In the RFOT the effective free energy barrier is characterized by a diverging length scale associated with the amorphous order [26, 29, 54, 55] or the correlated dynamics [56–59]. According to the RFOT, therefore, regardless of the fragility of liquids, a significant increase in τ_α should be universally described in terms of the growth of length scales. Testing this prediction of RFOT using Wigner glasses as an example of soft glasses with a broad range of tunable fragility is also an important motivation of this work.

METHODS

Interaction potential: Nearly four decades ago, Lindsay and Chaikin showed that increasing the volume

fraction of binary mixtures of highly charged micrometer-sized colloidal particles results in Wigner glass formation, characterized by the absence of long-range order but with finite shear modulus [20]. Following our previous studies [60, 61], we model the experimentally probed system as a mixture of charged spheres. The total number of the particles is $N = N_1 + N_2$, where N_1 and N_2 are, respectively, the number of small and large colloids. The bare radii of the particles, a_1 and a_2, are taken to be 0.525 μm and 1.1 μm, corresponding to the ones used in the experiments. In our simulations, we choose $N_1 = N_2 = 5000$. The interaction between the charged colloids is modeled by the Derjaguin-Landau-Verwey-Overbeek (DLVO) potential [62–66], which is given by,

$$V_{ij}(r) = \frac{e^2 Z_i Z_j}{4\pi\epsilon}\left(\frac{\exp[\kappa a_i]}{1+\kappa a_i}\right)\left(\frac{\exp[\kappa a_j]}{1+\kappa a_j}\right)\frac{\exp[-\kappa r]}{r}. \tag{1}$$

In Eq (1), Z_i is the valence of the charged colloids, whose values are 300 and 600 for small ($i = 1$) and large ($i = 2$) colloids, respectively, r is the inter particle distance, and ϵ is the dielectric constant ($\epsilon = \epsilon_0\epsilon_r$, where ϵ_0 and ϵ_r are vacuum and relative permittivity, respectively). Because the charged colloids are solubilized in water at temperature $T = 298K$, we use $\epsilon_r = 78$. The influence of the counterions and the added monovalent salt on the interaction between the charged colloids is implicitly reflected in the inverse Debye-Hückel screening length κ, given by,

$$\kappa^2 = \frac{e^2}{\epsilon k_B T}\left(\rho_c z_c^2 + \sum_{i'}^{n} \rho_{i'} z_{i'}^2\right), \tag{2}$$

where ρ_c and z_c are the number density and valence of the counterions, and k_B is the Boltzmann constant. For monovalent ions $|z_c| = 1$, and therefore due to charge neutrality ρ_c is given by $\rho_c = \rho_1 Z_1 + \rho_2 Z_2$, where ρ_1 and ρ_2 are the number densities of the small and large colloids, respectively. In Eq (2), $\rho_{i'}$ and $z_{i'}$ are the number density and valence of the added salt, respectively. For monovalent ions, $\sum_{i'}^{n} \rho_{i'} z_{i'}^2$ becomes $\rho_{add} = \sum_{i'}^{n=2} \rho_{i'}$. We define the relative number density of the excess ions as, $\rho_r = \rho_{add}/\rho_c$, and consider values of ρ_r ranging from 0 to 10. For simulation efficiency, $V_{ij}(r)$ is truncated and shifted at r_{cut} where $V_{ij}(r_{cut}) = 0.001 k_B T$. Because the interactions in Eq (1) are screened, it is not necessary to use Ewald sums, which is usually required for simulating systems with particles interacting by long-ranged Coloumb interactions. We investigated the dynamics of the charged colloids by carrying out extensive Brownian dynamics (BD) simulations, which we describe below (see Appendix A).

Softness of $V_{ij}(r)$: It is important to note that the *softness* of the interaction of the charged colloids varies with ρ_r and the volume fraction, $\phi = \frac{4\pi}{3L^3}(N_1 a_1^3 + N_2 a_2^3)$. We plot the DLVO potential $V_{11}(r)/k_B T$ for the small colloids as a function of r at different ϕ at $\rho_r = 0$ (Figure 1 (A)) and for different ρ_r at $\phi = 0.09$ (Figure 1 (B)). The graphs in Figures 1 (A) and (B) show that as ϕ and ρ_r decrease, the stiffness of the DLVO potential decreases, which means that $V_{11}(r)/k_B T$ decays less steeply as r increases. The effective range of the repulsive interaction increases as ϕ and ρ_r decrease. We use steepness and the range of the DLVO potential to characterize the changes illustrated in Figure 1 (A) and (B). The stiffness of the DLVO potential can be estimated as a slope of the interaction between colloidal particles as a function of r. Since the force is the negative slope of the potential, we define the stiffness parameter k_{ij} as the magnitude of the force of the DLVO potential at $r = l_B$ where $V_{ij}(l_B) = k_B T$. The Debye-Hückel screening length $1/\kappa$ is a length scale over which the electrostatic interaction of the charged colloids is effectively screened by other ions. Thus, the effective range λ_{DLVO} is $1/\kappa$. In Figures 1 (C) and (D), k_{DLVO} and λ_{DLVO} are shown for the range of ϕ considered in our simulations with varying ρ_r, respectively. For a fixed value of ρ_r stiffness k_{11} increases dramatically as ϕ increases (Figure 1). Because such changes in the interactions can be readily achieved in experiments, we can use charged colloidal suspensions to investigate how the nature of glass transition itself changes as ϕ and ρ_r are varied.

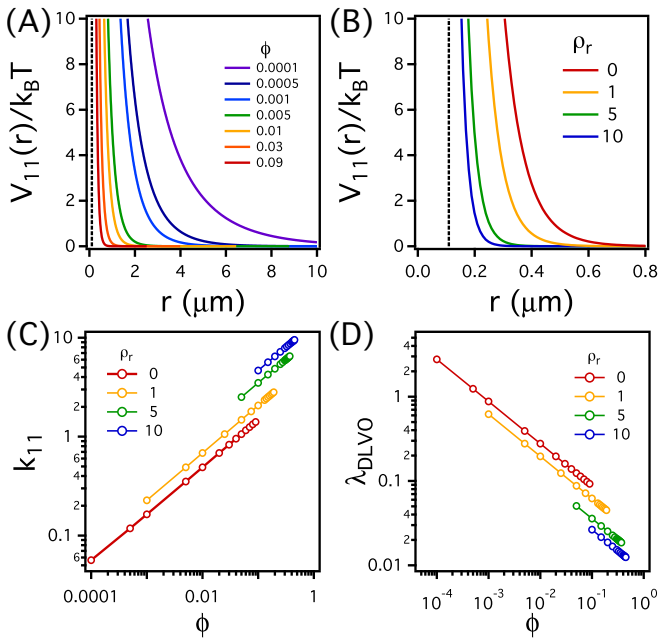

FIG. 1. **Variation in the softness of the interparticle potential of the charged colloids as a function of added salt.** Plot of the DLVO potential (Eq (1)) of the small charged colloids $V_{11}(r)/k_B T$ as a function of r (A) for various ϕ at $\rho_r = 0$, and (B) for various ρ_r with fixed $\phi = 0.09$. (C) The stiffness parameter of the small charged colloids k_{11}, and (D) the effective length scale of the DLVO potential λ_{DLVO} as a function of ϕ for various ρ_r. k_{11} in (C) is reduced by $k_B T/2a_1$. The unit of λ_{DLVO} in (D) is micrometer (μm).

RESULTS AND DISCUSSION

Two transition densities in Wigner glasses

In order to extract the structural relaxation times as a function of ϕ and ρ_r, we calculated the self-part of the intermediate scattering function,

$$F_q(t) = \frac{1}{N}\Big\langle \sum_{j=1}^{N} \exp\big[-i\vec{q}\cdot(\vec{r}_j(t)-\vec{r}_j(0))\big]\Big\rangle. \quad (3)$$

We used the wavenumber $q = |\vec{q}| = q_{ave} = \frac{2\pi}{d_{ave}}$, where $d_{ave} = 2\frac{\phi_1 a_1+\phi_2 a_2}{\phi_1+\phi_2}$, is the volume averaged diameter of the charged colloids with ϕ_1 and ϕ_2 being the volume fractions of the small and large colloids, respectively. The reason for using q_{ave} is that that the relaxation times extracted from the time-dependence of $F_{q_{ave}}(t)$ correlates well with the shear viscosity as a function of ϕ (see Appendix B). In Figure 2 (A), we plot the time dependence of $F_{q_{ave}}(t)$ as a function of ϕ at $\rho_r = 0$. As ϕ increases, there is a clear two-step decay in $F_{q_{ave}}(t)$, indicating that the dynamics of the charged colloids becomes glassy as the system is compressed. In Figure 2 (B), we show $F_{q_{ave}}(t)$ for various ρ_r at a fixed $\phi = 0.15$. As ρ_r decreases, the effective range of the repulsive interaction of the charged colloids increases (Figure 1 (B) and (D)), which results in an increase in the effective density of the charged colloids, thus explaining the sluggish dynamics with decreasing ρ_r (Figure 2 (B)).

As stated in the Introduction, a key prediction of RFOT is that for a generic glass forming materials that undergo SGT as it is compressed (or supercooled), there are two characteristic transitions. One of them is expected at $\phi = \phi_d$, denoting the start of dynamical arrest. The other is the ideal glass transition at ϕ_K, which is usually difficult to probe in computer simulations. The onset of sluggish structural relaxation dynamics in Figure 2 (A) and (B) can be quantified by an increase in the structural relaxation time, τ_α. For practical purposes, we calculated τ_α using $t = \tau_\alpha$ at which $F_{q_{ave}}(\tau_\alpha) = 0.2$. The dependence of τ_α as a function of ϕ for various ρ_r is shown in Figure 2 (C). In the ϕ and ρ_r range considered here, τ_α for a given ρ_r, increases by nearly 4 orders of magnitude as ϕ increases.

We analyzed the growth in τ_α with ϕ in terms of the two characteristic transition densities [1, 7]. As ϕ approaches ϕ_d an extensive number of metastable glassy states emerge. At densities above ϕ_d the system is trapped in one of the many metastable states for arbitrarily long times, and transport occurs through activated transitions involving crossing growing free energy barriers. The free energy barrier $\Delta F^{\ddagger}$ between two adjacent mosaic states scales as the size of the mosaic states ξ, and is given by $\Delta F^{\ddagger} \sim \xi^{d/2}$, where d is the space dimension. The RFOT theory predicts that ξ should increase without bound as $\phi \to \phi_K$ ($\xi \sim (\phi_K - \phi)^{-2/d}$), which in turn leads to the essential singularity in τ_α at ϕ_K.

The values of ϕ_d and ϕ_k can be extracted using the data in Figure 2 (C). The dynamical transition anticipated in the RFOT theory is consistent with the prediction of the mode-coupling theory (MCT), with the caveat that the power law singularity is avoided in reality. We calculated ϕ_d using $\tau_\alpha \sim (1-\phi/\phi_d)^{-\gamma}$, where ϕ_d and γ are the fitting parameters. The values of γ for $\rho_r = 0$ and 1 are unusually large (Table 1) especially at low salt concentrations. This could arise because the estimated ϕ_d may already be in the activated regime. It is difficult to calculate τ_α accurately at zero and low salt concentrations over a broad enough range of ϕ to accurately in order to estimate both ϕ_d and γ unambiguously. This is likely due to the long range of the DLVO potential especially when ρ_r=0.

As the density is increased further, τ_α follows the Vogel-Flucher-Tamman (VFT) relation,

$$\tau_\alpha = \tau_{VFT} \exp\Big[\frac{D_{VFT}\phi}{\phi_K - \phi}\Big], \quad (4)$$

where τ_{VFT} is τ_α for $\phi \to 0$, and D_{VFT} is the fragility parameter. We fit τ_α to the VFT relation in order to extract τ_{VFT}, D_{VFT} and ϕ_K. Note that the asymptotic behavior predicted by the RFOT is well described with a single value of ϕ_K obtained by a VFT fit (see below), which partly validates our determination of ϕ_K. The dashed and solid lines in Figure 2 (C) represent the power laws and the VFT fits. The significant increase in τ_α is accurately fit by the two functional forms in different ranges of ϕ.

In Figure 2 (D), we show ϕ_d and ϕ_K for various ρ_r (see the values in Table 1). Interestingly, as ρ_r increases from 0 to 10, ϕ_d and ϕ_K increase from 0.10 and 0.22 to 0.46 and 0.50, respectively. Considering that upon an increase in ρ_r, the shape of the DLVO potential becomes more hard sphere-like (see Figure 1 and Appendix C), we expect that ϕ_d and ϕ_K should converge to the values for binary hard spheres ($\phi_d \simeq 0.59$ and $\phi_K \simeq 0.64$ [67]) at high values of ρ_r. The results in Figure 2 (D) show that ϕ_d and ϕ_k indeed increase. However, the numerical values for Wigner glasses and HS differ, which is related to the range of the DLVO potential. We showed sometime ago that pair correlation functions of highly charged spherical colloidal suspensions with bare size a can be mapped onto hard spheres with diameter d_h that is greater than a [65, 68]. Thus, a similar mapping would predict that the volume fractions identified here would be larger if the effective hard sphere diameters are used. With this argument, we conclude that the effective ϕ_K for Wigner glasses at high ρ_r would achieve the well-known values for hard sphere systems. The distances $(\phi_K - \phi_g)/\phi_K$ at $\rho_r = 10$ (Figure 2 (D)) and for hard sphere-like are virtually identical, which is also manifested in the fragile-strong crossover (see below). It is clear that addition of

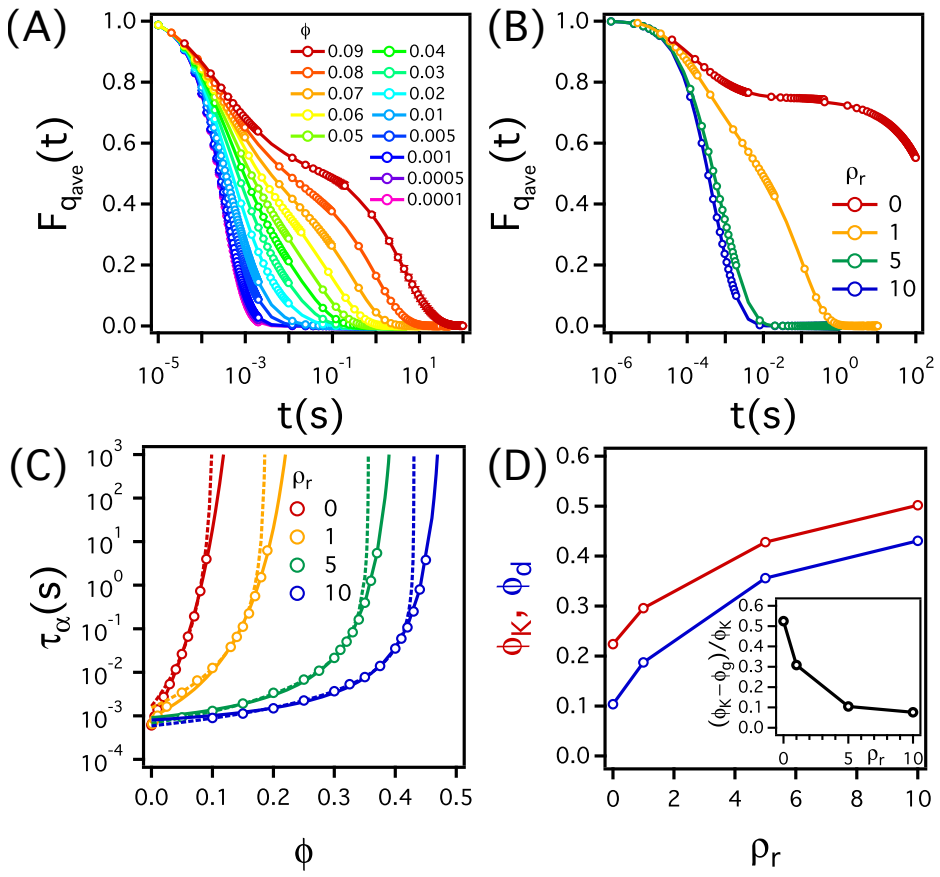

FIG. 2. **Structural relaxation and glass transition in charged colloids.** The self-part of the intermediate scattering function $F_{q_{ave}}(t)$ (A) for various ϕ with $\rho_r = 0$ and (B) for various ρ_r with $\phi = 0.15$. (C) The relaxation time of the charged colloids as a function of ϕ for various ρ_r. The solid and dashed lines indicate VFT and MCT fits to τ_α, respectively. (D) The characteristic densities ϕ_K (red circles) and ϕ_d (blue circles) as a function of ρ_r.

salt influences the softness of the DLVO potential, which drastically alters the glass transition behavior.

Fragility decreases substantially as ρ_r decreases

The variations in the fragility can be visualized using the Angell plot, from which the fragility index may be calculated by fitting τ_α on a logarithmic scale with respect to ϕ/ϕ_g where ϕ_g is the volume fraction at the glass transition. The difference between strong and fragile glasses is evident in the dependence of τ_α, which increases gradually as ϕ/ϕ_g increases for strong glass formers, but for fragile glass formers the increase is steep. It is worth emphasizing that substantial variations in the curvatures observed in the dependence of τ_α on ϕ (Figure 2(C)) is observed in experiments only when shear viscosity for a very large class of materials as a function of temperature is simultaneously plotted. Remarkably, here in binary mixture of charged suspensions, interacting with isotropic DLVO potential, a similar behavior is observed. The results in Figure 2(C) allows us to construct the Angell plot, τ_α versus ϕ/ϕ_g where ϕ_g is the glass transition density.

In order to obtain the Angell plot for Wigner glasses, we first determined ϕ_g for various ρ_r, which is not a trivial task in the simulations. Typically, ϕ_g is obtained from experimental data using $\tau_\alpha(\phi_g) = 100s$. For colloidal systems, when $\tau_\alpha = 100s$, $\tau_\alpha/\tau_{VFT} \simeq 10^5$, thus ϕ_g can be obtained using $\tau_\alpha(\phi_g)/\tau_{VFT} = 10^5$ [36, 37]. In order to calculate ϕ_g, therefore, one should consider the range of ϕ where $\tau_\alpha \simeq 100s$ or $\tau_\alpha/\tau_{VFT} \simeq 10^5$, which, unfortunately, is not practical using computer simulations. Alternatively, assuming that τ_α for high ϕ regime follows the VFT relation (Eq 4), we determined ϕ_g by extrapolating Eq 4 to ϕ where $\tau_\alpha/\tau_{VFT} = 10^5$ (see Table 1). The values of τ_α at ϕ_g for various ρ_r in our simulations are $\sim 100s$, which justifies our estimation of ϕ_g.

The Angell plot for charged colloids for various ρ_r values are shown in Figure 3 (A). We expect τ_α for strong glasses to increase linearly as a function of ϕ/ϕ_g [35, 36], which implies that $\tau_\alpha \sim \exp[A\phi]$ (the red dashed line

	MCT		VFT			
ρ_r	ϕ_d	γ	τ_{VFT}	ϕ_K	D	ϕ_g
0	0.10±0.03	4.215±0.0003	0.8±0.1 $\times 10^{-3}$	0.20±0.02	10±2	0.11
1	0.187±0.006	2.7±0.3	1.7±0.2 $\times 10^{-3}$	0.264±0.006	3.2±0.3	0.20
5	0.356±0.003	1.9±0.1	0.9±0.1 $\times 10^{-3}$	0.429± 0.004	1.4±0.1	0.38
10	0.431±0.001	1.55±0.03	0.79±0.07 $\times 10^{-3}$	0.502±0.004	0.97±0.07	0.46

TABLE I. Characteristic volume fractions associated with compressed charged colloids

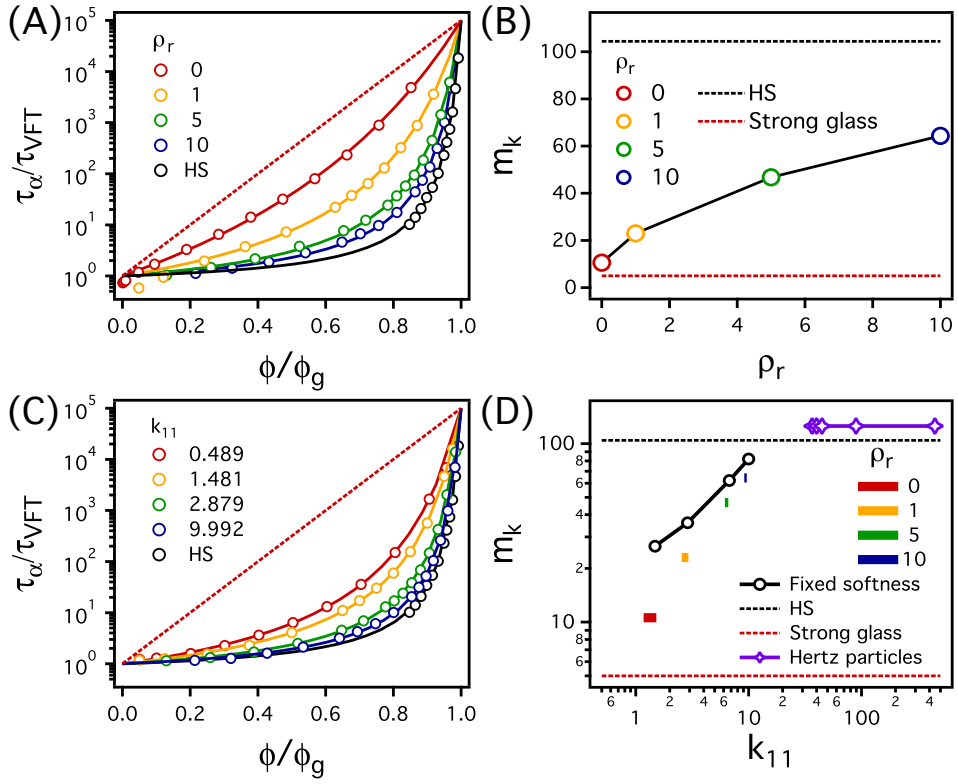

FIG. 3. **Variations in the fragility of charged colloids.** (A) Angell plot in which τ_α for various ρ_r is shown as a function of ϕ/ϕ_g. The black open circles (the rightmost curve) are τ_α of ϕ for hard spheres. The red dashed line shows the Angell plot for a strong glass. The solid lines are the corresponding VFT fits. (B) The fragility index m_k as a function of ρ_r. The red and black dashed lines show the fragility of the strong glass and hard spheres, respectively. (C) Relaxation time as a function of as a function of ϕ/ϕ_g with the stiffness k_{11} explicitly shown. (D) Fragility index as a function of k_{11}. For comparison we also show m_k (Eq. (5)) for a few other systems.

in Figure 3 (A)), where A is a constant (the red dashed guide line). On the other hand, for hard sphere colloids that we consider as a reference for a fragile glass (Appendix D), τ_α increases rapidly as ϕ/ϕ_g approaches 1 (the black circles). Figure 3 (A) shows that the slope of τ_α near $\phi/\phi_g = 1$ increases significantly as ρ_r increases, indicating that the fragility increases with ρ_r. We quantify the fragility change using the *kinetic fragility index* m_k, which is defined as,

$$m_k = \frac{d \log \tau_\alpha}{d\phi/\phi_g}\Big|_{\phi=\phi_g}. \quad (5)$$

For a strong glass, $m_k = 5$ since $\log[\tau_\alpha/\tau_{VFT}]$ is linear in ϕ/ϕ_g (the red dashed line in Figure 3 (B)) [36]. The value of m_k in the hard sphere limit is 104 (the black dashed line in Figure 3 (B)). The calculated m_k values of the charged colloids using Eq (5), displayed in Figure 3 (B), shows that m_k increases from 10 to 64 as ρ_r increases from 0 to 10. Since the DLVO potential approaches the hard sphere potential as ρ_r increases (see Appendix C), it is likely that if ρ_r is increased further, m_k would converge (perhaps slowly) to the values associated with hard sphere glasses. Therefore, our simulation results demonstrate that by merely tuning the salt concentration, m_k of the charged colloids can be changed dramatically. In other words, addition of a monovalent salt could result in

the fragile-strong crossover in Wigner glasses, which is a prediction that can be readily validated experimentally.

Stiffness of the DLVO potential and dramatic fragility changes

Significant changes in m_k for soft colloids have been reported previously [35, 40–42], but the physics underlying this behavior in terms of the interparticle interaction has remained unclear, and perhaps even controversial. It was found that there is a crossover from fragile to strong glasses in deformable microgels when the internal elasticity of the particles decreases. This finding was used to suggest that softer potentials should result in strong glasses [35]. However, the drastic variations in m_k have not been reproduced in previous simulations by modification of the softness of the potential alone [37, 47–49]. For instance, Philippe et al., considered the soft particles interacting via the Hertz potential $V_H(r) = \epsilon_H(1 - r/\sigma)^2\Theta(r - \sigma)$, where $\Theta(x)$ is the Heaviside step function, and σ is the diameter of the particles [37]. The softness of the potential was tuned by the value of ϵ_H. Although ϵ_H was varied by two orders of magnitude, the dependence of τ_α on ϕ was found to be insensitive to ϵ_H (Figure 3 (D)). This implied that the fragility is independent of the softness of the Hertz potential. Thus, they concluded that the idea the softness of the potential solely controls the fragility should be revised.

Our results for the glass transition of the charged colloids provide insights into these seemingly conflicting arguments. As shown in Figure 1 (B), the DLVO potential becomes soft as ρ_r decreases, but even at $\rho_r = 0$ the stiffness is altered significantly by ϕ. These two features of the DLVO potential should contribute to the drastic change in m_k with ρ_r in Figure 3 (B). In order to distinguish between the influence of the softness from that of the other, we carried out additional simulations for the charged colloids whose value of κ in Eq (2) is fixed as a function of ϕ. Note that the softness parameter k_{11} and λ are determined by κ. When κ is fixed, therefore, the shape (and thereby softness of the potential) is not changed with ϕ. Accordingly, if the fragility varied with κ (or associated softness parameters k_{11} and λ), this would be attributed solely to the stiffness of the potential.

Figure 3 (C) shows the Angell plots for various k_{11}, from which we evaluate m_k as a function of k_{11} in Figure 3 (D) (the black open circles). They clearly show that as k_{11} decreases (as the potential becomes softer), m_k decreases. Therefore, from Figure 3 (D) we conclude that soft potentials (smaller values of k_{11}) can indeed make glass transition stronger.

More importantly, the softness of the potential is insufficient to fully explain the drastic modification of the fragility shown in Figure 3 (B). We show m_k for various ρ_r in the y axis of Figure 3 (D) (the horizontal color bars) and the x range of each color bar represents the range of $1/k_{11}$ from ϕ_g to $\phi = \phi_{ref}$ at which $\tau_\alpha/\tau_{VFT} = 10^2$. Note that the x axis is drawn in a log scale, and thus the range of the color bars in the graph indicates the extent of how sensitively k_{11} changes relatively to k_{11,ϕ_g} when ϕ drops from ϕ_g to ϕ_{ref}. The graph shows that as ρ_r decreases, k_{11} varies more with ϕ and m_k drops further from that of the hard sphere (the black dashed line) comparing to when the softness is fixed with ϕ (the black circles). This demonstrates that the variation of the softness with ϕ should also play an important role in the drop of the fragility with a decrease in ρ_r.

Note that the potential of the deformable microgels in previous experiments would behave in a similar way upon packing. The microgels deswell significantly upon packing due to their polymeric nature, leading to a decrease in the effective size and an increase in the internal elasticity [36]. This may alter the shape of the potential becoming steeper with increasing ϕ, which is qualitatively similar to the DLVO potential. When deswelling upon packing was limited, the fragility of the migrogels was insensitive to the softness of the potential [36]. Therefore, it was suggested recently that rather than softness itself, such variation in the shape of potential with ϕ would play a more dominant role in the change in m_k of the microgels [36, 37].

Figure 3 (D) partly supports this idea. Typical soft microgels in experiments are modeled using the Hertz potential with $\epsilon_H/k_BT \simeq 1000$ [69, 70],which corresponds to $k_{11} \simeq 60$, where k_{11} of the Hertz potential is expressed as $k_{11} = 2\sqrt{\epsilon_H/k_BT}$. In Figure 3 (D) we show m_k for the Hertz particles as a function of k_{11} considered in the previous simulation of Philippe et al. [37] (the purple open stars). The considered range of ϵ_H/k_BT is from 333 to 50000, which corresponds to k_{11} in the range from 36 to 447. The m_k values for the Hertz particles is obtained as $m_k \simeq 125$ from the simulation data in [37], which is independent of k_{11}. Thus, $k_{11} \simeq 60$, which is steep resulting in the glass transition being more fragile according to Figure 3 (D). This means that the drastic decrease in m_k in microgels could be attributed to other mechanisms associated with their deswelling. However, further investigation is needed to elucidate how much the potential of the microgels is modified by deswelling and whether this change in the potential contributes to the fragility of the microgels.

To conclude this section, we showed that the fragility of the charged colloids decreases drastically as ρ_r decreases. As ρ_r decreases, the DLVO potential becomes softer, changing sensitively with ϕ, which are the determining factors in the decrease in m_k of the charged colloids. Although our results confirm that the softness of the potential can reduce the fragility it is not a unique contribution to drastic change of the fragility observed in the previous experiments. As a result, the conclusion of the pioneer-

ing experiment [35] should be revisited. *The soft nature of inter particle potential is sufficient but not necessary in order to observe a broad change in the fragility, which is a reflection of the dependence of the relaxation times on ϕ.*

RFOT quantitatively accounts for glass transition in charged colloids

In previous sections, we showed that the nature of glass transition in charged colloids is modified by the addition of monovalent salts. In particular, as ρ_r increases, ϕ_K increases and τ_α increases more steeply as $\phi \to \phi_K$. In this section, we explore the extent to which the universal aspects of RFOT are manifested in Wigner glasses. We find evidence for strong spatial heterogeneity in the dynamics of the charged colloids as ϕ approaches glass transition. We also demonstrate that *dynamic heterogeneity* is closely associated with a significant increase in τ_α, which is a consequence of the increase in length scale as the system is compressed, which was anticipated by the RFOT for the SGT problem.

As ϕ increases above ϕ_d, the dynamics of supercooled liquids becomes spatially heterogeneous, which implies that particles with similar mobilities are likely to be localized close to each other. Spatial heterogeneity, resulting in violation of law of large numbers [7, 61, 71], is one of the most striking features of the glass transition [72–74]. The heterogeneous dynamics in Wigner glasses is pictorially illustrated in Figure 4 (A). We prepared the simulation snapshots at values of ϕ from $\phi = 0.3$ to $\phi = 0.45$ at $\rho_r = 10$. We colored the individual particles according to their relative mobility M_i defined as $M_i = \Delta r_i^2(\tau_{d_{ave}})/\langle \Delta r^2(\tau_{d_{ave}})\rangle$, where $\Delta r_i(t)$ is the displacement of particle i at time t, and $\tau_{d_{ave}}$ is a timescale at which the mean-squared displacement $\langle \Delta r^2(\tau_{d_{ave}})\rangle$ is equal to d_{ave}. Note that $\tau_{d_{ave}}$ is comparable to the structural relaxation time τ_α, indicating that the structural correlation of whole system would be vanishingly small at $\tau_{d_{ave}}$. A typical liquid is ergodic on the observation time scales τ_{obs} that is comparable to τ_α. Thus, the structural correlation in liquids in any large enough subsample would fully vanish for τ_α. As $\phi \to \phi_d$, however, the system becomes non-ergodic even on $\tau_{obs} \gg \tau_\alpha$ due to the emergence of an ensemble of disconnected mosaic states. As a consequence, relaxation becomes spatially heterogeneous over large regions. Thus, as $\phi \to \phi_d$, the mobilities of the particles are spatially heterogeneous and many of the particles in certain regions rarely diffuse. This reveals that the time evolution of the particles varies from region to region even if $\tau_{obs} \simeq \tau_{d_{ave}}$. This is a clear indication of the dynamic heterogeneity and is a consequence of broken ergodicity near ϕ_d, which is an important consequence of the RFOT [7].

Fourth order susceptibility: The extent of dynamic heterogeneity can be quantified by the fluctuations in the two-point correlation function characterizing the structure relaxation. Hence, we should consider the four-point susceptibility, first introduced in [75], of the intermediate scattering function $\chi_{4|F_q}(t) = \frac{1}{N}[\langle F_q(t)^2\rangle - \langle F_q(t)\rangle^2]$. However, the fluctuation of the overlap function is often used as an alternative for numerical convenience, whose behavior is qualitatively similar to $\chi_{4|F_q}(t)$. The overlap function $F_o(t)$ is defined as,

$$F_o(t) = \frac{1}{N}\sum_{i=1}^{N} w_i(t), \tag{6}$$

where $w_i(t) = \Theta(a - |\vec{r}_i(t) - \vec{r}_i(0)|)$ and $\Theta(x)$ is the Heaviside step function, which accounts for the fraction of the slow particles that diffuse a distance less than a. If one uses $a = 0.3d_{ave}$, $F_o(t)$ behaves in a qualitatively similar fashion to $F_{q_{ave}}(t)$ [57]. Thus, the overlap function can be used to quantify the structural relaxation of liquids instead of $F_{q_{ave}}(t)$. The four-point susceptibility of $F_o(t)$ for the N particle systems is expressed as,

$$\chi_{4|F_o,N}(t) = N[\langle F_o(t)^2\rangle - \langle F_o(t)\rangle^2] \tag{7}$$

which characterizes the fluctuation of the slow particles. If the dynamics of liquids becomes spatially heterogeneous, $\chi_{4|F_o,N}(t)$ should have a large value. Accordingly, $\chi_{4|F_o,N}(t)$ can be used as a measure of the overall extent of dynamic heterogeneity. In Figure 4 (B), we plot $\chi_{4|F_o,N}(t)$ as a function of t for various values of ϕ at $\rho_r = 0$, $a = 0.3d_{ave}$ and $N = 10,000$. $\chi_{4|F_o,N}(t)$ has a maximum value near $t = \tau_{ov}$, which is the relaxation time of $F_o(t)$ defined as t at which $F_o(t) = 0.2$. An increase in ϕ results in the maximum value increasing drastically, showing the growth in the extent of dynamic heterogeneity as ϕ approaches the glass transition.

It should be noted that $\chi_{4|F_o,N}(t)$ obtained directly from Eq (7) in simulations is subject to strong finite size effects, because the contribution of long-range density fluctuations over the length scale L (the simulation box size) to $\chi_{4|F_o,N}(t)$ is not included [57]. A more exact estimation of the extent of dynamic heterogeneity can be achieved by the small wavenumber behavior of the four-point dynamic structure factor $S_4(q,t)$ defined as,

$$S_4(q,t) = N[\langle W_o(q,t)W_o(-q,t)\rangle - \langle W_o(q,t)\rangle^2], \tag{8}$$

where $W_o(q,t) = \frac{1}{N}\sum_{j=1}^{N} w_j(t)\exp[-i\vec{q}\cdot\vec{r}_j(0)]$. For small q, $S_4(q,t)$ can be fit by the Ornstein-Zernicke equation [57, 59, 76, 77],

$$S_4(q,t) \simeq \frac{\chi_{4|F_o,\infty}(t)}{1 + (q\xi_{4|F_o}(t))^2} \quad \text{for } q \to 0, \tag{9}$$

where $\chi_{4|F_o,\infty}(t)$ is $\chi_{4|F_o,N}(t)$ of an infinitely large system and $\xi_{4|F_o}(t)$ is a length scale of dynamically correlated regions, both of which can be determined as fitting parameters. The results are shown in Figure 4 (C).

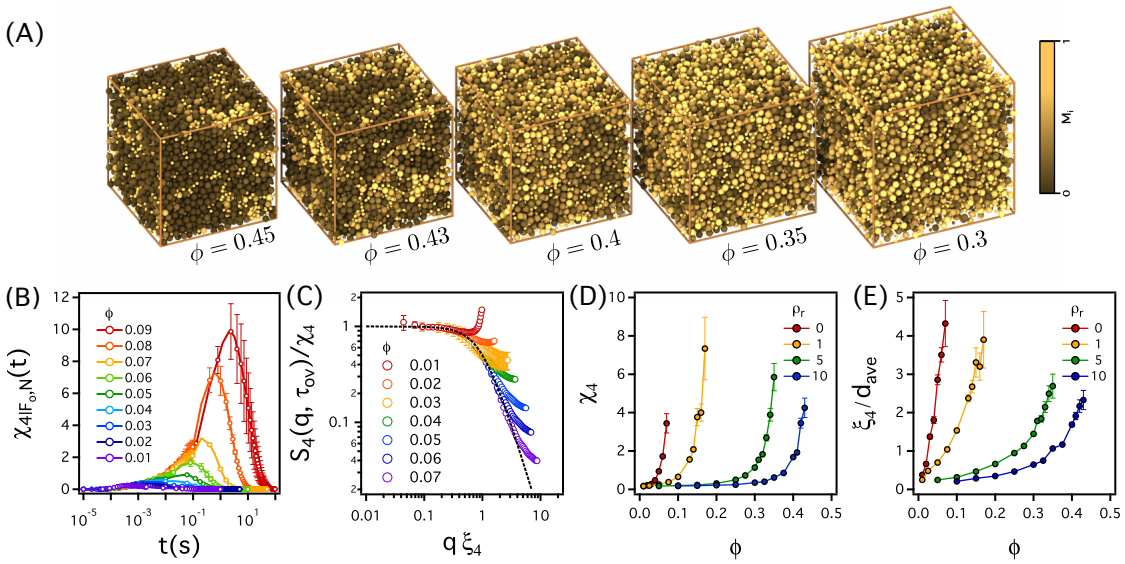

FIG. 4. **Visualization and quantification of heterogeneous dynamics in charged colloids.** (A) Snapshots illustrating heterogeneous dynamics. Equilibrium configurations for various ϕ with $\rho_r = 10$ are prepared. Coloring of the colloids are done according to their relative mobility M_i (see the definition of M_i in the main text). (B) The four-point susceptibility of the overlap functions $\chi_{4|F_o,N}(t)$ for various ϕ at $\rho_r = 0$. (C) The rescaled four-point structure factor $S_4(q,t)/\chi_4$ with respect to the reduced wavenumber ξ_4 when $t = \tau_{ov}$ and $\rho_r = 0$. The dashed line represents Ornstein-Zernicke fit, $S_4(q, \tau_{ov})/\chi_4 = 1/[1 + (q\xi_4)^2]$. (D) χ_4 and (E) ξ_4 of the charged colloids versus ϕ for various ρ_r.

The values of $\chi_{4|F_o,N}(t)$ and $\xi_{4|F_o}(t)$ are maximized near τ_{ov} [57], allowing us to determine the dynamic susceptibility and the associated length scale of the charged colloids as $\chi_4 = \chi_{4|F_o,N}(\tau_{ov})$ and $\xi_4 = \xi_{4|F_o}(\tau_{ov})$, respectively. Figures 4 (D) and (E) provide a quantitative illustration of the growing dynamic heterogeneity of the charged colloids. They show that χ_4 and ξ_4 increase as ϕ approaches the glass transition density, implying that a significant slowdown of dynamics near the glass transition is accompanied by heterogeneous dynamics of the charged colloids. Note that the magnitudes of such multi-point dynamic susceptibility ξ and the associated length scale ξ are quantities associated with the magnitude of the effective energy barrier of the structural relaxation, indicating that the increase in χ_4 and ξ_4 leads to orders of increase in τ_α . Below, we establish a casual relationship between dynamic heterogeneity and sluggish dynamics of Wigner glasses using the RFOT theory.

Fractal dimension of dynamically correlated regions: The RFOT theory provides a comprehensive explanation on how the growth of ξ_4 and χ_4 correlates with a sluggish dynamics of the charged colloids. It predicts that as ϕ increases beyond ϕ_d the nature of the nature of the configurational space partitions into an exponential number of mosaic states. Further compression results in the power law divergence of ξ close to ϕ_K, which leads to a dramatic increase in τ_α. Since the physical origin of dynamic heterogeneity is closely associated with the emergence of the mosaic states, it is natural to expect that the properties of the dynamically correlated regions characterized by ξ_4 and χ_4 to be consistent with those of the mosaic states. This implies that the increase of τ_α should be described by the growth of ξ_4 as the system is compressed.

Although it is unclear if ξ_4 behaves in a qualitatively similar way as ξ [78], many theoretical studies have shown that the growth of ξ_4 plausibly captures the important aspects of the RFOT associated with the mosaic states [56–59, 79, 80]. For example, according to the RFOT theory, the shape of the mosaic states is string-like but would become compact as $\phi \to \phi_d$, which can be captured by the change in the shape of the dynamically correlated domains [81]. Since χ_4 is often interpreted as the number of particles in the dynamically correlated domains [82, 83], it follows that if χ_4 is plotted with respect to ξ_4 in a log-log scale, the exponent should be associated with the fractal dimension d_f of the dynamically correlated domains. Therefore, if the transition of the shape of the dynamically correlated regions were associated with the mosaic states, d_f should increase to 3 as $\phi \to \phi_d$, and ϕ exceeds ϕ_d. Flenner et al. computationally showed that the transition in d_f of various types of model glasses occurred universally as ϕ (or T) approached the dynamic transition points ϕ_d (or T_d) [58]. We observe a similar universal transition in d_f in the charged colloidal glasses. Figure 5 (A) shows χ_4 as a function of ξ_4 for various ρ_r values. As shown in the graph, χ_4 vs ξ_4 for various ρ_r collapses on to a single curve using an appropriate rescaling

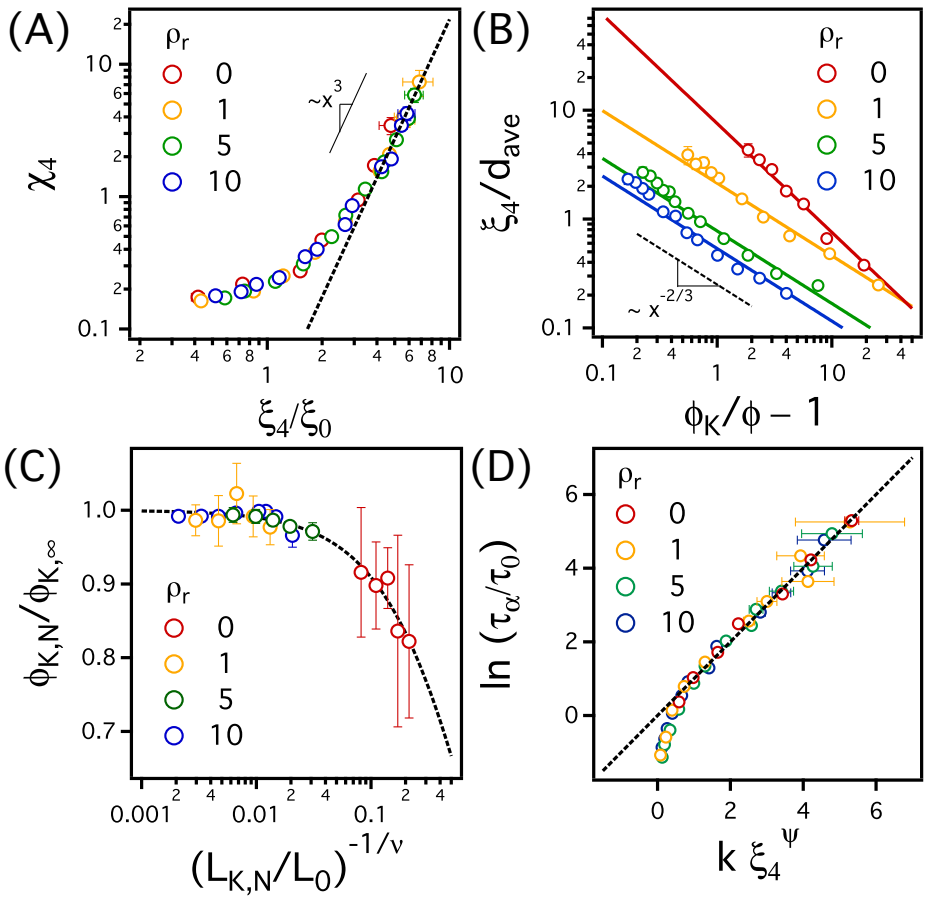

FIG. 5. **Illustrating RFOT behavior in charged colloids.** (A) χ_4 for various ρ_r values as a function of ξ_4 extracted using Eq. (9). The values of ξ_0 for various ρ_r are determined to make all the data points collapse onto a single curve for clarity, which does not influence the scaling relation between ξ_4 and χ_4. The dashed line ($y \sim x^3$) is drawn as a guide to the eye. (B) ξ_4 for the various ρ_r as a function of $\phi_K/\phi - 1$. For ρ_r the largest ϕ for which reliable simulations could be done is less than ϕ_g (see Figure 2 (C)), which is a great distance away from the extrapolated ϕ_K value (Table 1), which is outside the regime of applicability of the RFOT theory. The exponent $-2/3$ holds for $\rho_r = 1$, 5, and 10. (C) Dependence of the reduced ideal glass transition volume fractions $\phi_{K,N}/\phi_{K,\infty}$ on the system size N are shown as $(L_{K,N}/L_0)^{-1/\nu}$ is varied. The dashed line ($\phi_{K,N}/\phi_{K,\infty} - 1 = (L_{K,N}/L_0)^{-1/\nu}$) validates that the finite size scaling relation predicted by the RFOT theory. Individual fits are shown in Figure 10 in Appendix F. (D) The logarithm of the relaxation time $\ln \tau_\alpha$ with respect to ξ_4^ψ. The dashed guide line ($y = x$) confirms the linear relation between the two quantities.

factor ξ_0, and d_f increase to 3 as $\phi \to \phi_d$. This particular example confirms the relevance between the dynamically correlated domains and the mosaic states, which guarantees that the growth of ξ_4 with ϕ characterize the dependence of ξ on ϕ.

Increase in length scale upon compression: According to the RFOT theory [1, 7], ξ should grow as $\phi \to \phi_K$,

$$\xi \sim \left(\frac{\phi_K}{\phi} - 1\right)^{-\nu}, \tag{10}$$

where $\nu = \frac{2}{d}$ is the scaling exponent. We confirm that this is indeed the case when ξ_4 is plotted as function of ϕ. We use ϕ_K obtained in Figure 2 (C) and (D), and plot ξ_4 for various ρ_r with respect to $\phi_K/\phi - 1$ in Figure 5 (B). The slopes of the linear guide lines in the graph represent the values of ν which are expected to be $2/d$ by the RFOT theory. For ρ_r =1, 5, and 10, ξ_4 of ϕ follows well Eq 10 with $\nu = 2/3$. For completeness, we also plot the results for $\rho_r = 0$. In principle, Eq (10) is applicable only if ϕ is relatively close to ϕ_K. For $\rho_r = 0$, the distances ($\Delta\phi_K = 1 - \phi/\phi_K$) between ϕ_K and the maximum ϕ_{max} for which reliable simulations can be performed (Figure 5 (B)) is 0.65, which is two to four times larger than for $\phi_r = 1$, 5, and 10. This results in the deviation from the expected value in ν when $\rho_r = 0$. Thus, to more precisely determine ν for $\rho_r = 0$, it is necessary to estimate ξ_4 at larger values of ϕ, which is difficult to do in simulations. Nevertheless, the results in Figure 5 (B) are sufficient to demonstrate that, as predicted by RFOT, ξ_4 for various

ρ_r of the charged colloids would diverge at ϕ_K, thus validating one of the key predictions of the RFOT theory.

In order to show that the divergence of τ_α at ϕ_K is due to the increase in $\xi \simeq \xi_4$, we investigated the finite size effects on the estimates of ϕ_K. Let us assume that the system with size L is a subsample of an infinitely large system whose ϕ_K is $\phi_{K,\infty}$. Then, ϕ_K of L would be determined as ϕ at which $\xi_4 \simeq L$. Therefore, ϕ_K and L of the subsystems would follow Eq 10 with respect to $\phi_{K,\infty}$, which leads to the finite size scaling relation of ϕ_K,

$$L \sim \left(\frac{\phi_{K,\infty}}{\phi_{K,L}} - 1\right)^{-\nu}, \tag{11}$$

where $\phi_{K,L}$ is ϕ_K of the subsystem of size L. When N is fixed, as in our simulation, L is a function of ϕ, $L_N \sim (N\phi)^{-1/3}$. Hence, for constant N system, $\phi_{K,N}$ would coincide with ϕ, which is determined using $\xi \simeq L_{N,K} \sim (N\phi_{K,N})^{-1/3}$. This leads to $L_{K,N} \sim (\phi_{K,\infty}/\phi_{K,L} - 1)^{-\nu}$, from which $\phi_{K,N}$ can be expressed as a function of $L_{K,N}$ as below,

$$\phi_{K,N} = \frac{\phi_{K,\infty}}{1 + \left(\frac{L_{K,N}}{L_0}\right)^{-1/\nu}}, \tag{12}$$

where $\phi_{K,N}$ indicates ϕ_K associated with finite N and we define $L_{K,N}$ as $L_{K,N} = (N/\phi_{K,N})^{1/3}$. We carried out additional simulations for various N and estimated $\phi_{K,N}$ using the VFT relation as done in Figure 2 (C). Then, L_0 and $\phi_{K,\infty}$ are determined as fitting parameters in Eq (12) (see details in Appendix F). For the purpose of fitting the curves, $\nu = 2/3$ is used for $\rho_r = 1, 5$, and 10, but we use an effective value $\nu = 1$ for $\rho_r = 0$. Figure 5 (C) shows that $\phi_{K,N}/\phi_{K,\infty}$ for various ρ_r collapses onto a single curve ($y = (1+x)^{-1}$) when plotted against $L_{K,N}^{-1/\nu}$, indicating that $\phi_{K,N}$ follows the scaling relation in Eq 12. This clearly demonstrates that it is the growth of ξ_4 that contributes to the slow dynamics of the charged colloids as ϕ_K is approached.

Free energy barrier and growing length scale: The quantitative relation between the growing length scale associated with dynamic heterogeneity and the slowing down of the structural relaxation in Wigner glasses can be explained using RFOT theory [1]. The activation free energy $\Delta F^\ddagger$ of a configuration to move from one mosaic state to another increases with an increase in the length scale associated with the mosaic states, i.e., $\Delta F^\ddagger \sim \xi^\psi$, where ψ is a scaling exponent. This implies that the structural relaxation time is related to ξ as,

$$\tau_\alpha = \tau_0 \exp[k\xi^\psi], \tag{13}$$

where τ_0 is a timescale at $\xi \to 0$ which is comparable to τ_{VFT} and k is a prefactor for $\Delta F^\ddagger$. Note that ψ is predicted to be $1/\nu$, such that by substituting ξ with Eq (10), Eq (13) can recover the VFT relation. We determine τ_0 and k at various values of ρ_r by fitting τ_α to Eq (13). Figure 5 (D) shows $\ln[\tau_\alpha/\tau_0]$ at various ρ_r values plotted against $k\xi_4^\psi$, where $\psi = 1/\nu$ in Figure 5 (B). The linear line ($y = x$) in the graph is drawn as a guide to confirm the quantitative consistency between the two quantities. This figure clearly illustrates that as $\phi \to \phi_K$, τ_α for Wigner glasses at various ρ_r values can be quantitatively described by Eq (13).

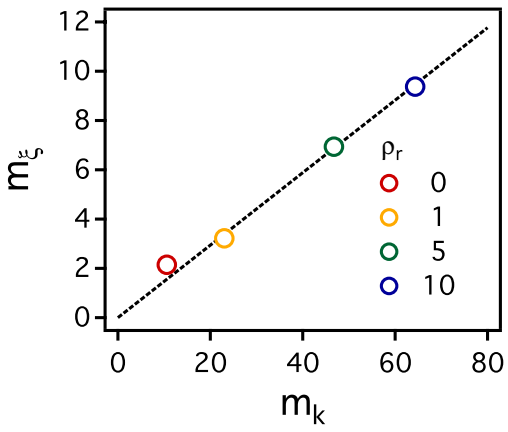

FIG. 6. **The linear relation between m_ξ and m_k.** m_ξ for the charged colloids as a function of m_k for various ρ_r. The dashed line in the graph confirms a linear relation between two quantities.

Analogies between Wigner and molecular glasses

We investigated how the growing length scale relates to the fragility of the charged colloids. By replacing τ_α in Eq (5) with Eq (13), we can define the fragility index m_ξ in terms of ξ, i.e.,

$$m_\xi = k\frac{d\xi^\psi}{d\phi/\phi_g}\Big|_{\phi=\phi_g}, \tag{14}$$

where ξ_{ϕ_g} is ξ at $\phi = \phi_g$. Since $k\xi_{\phi_g}^\psi = \ln[\tau_\alpha(\phi_g)/\tau_0]$ and $\tau_\alpha(\phi_g)/\tau_0 \simeq 10^5$ for the colloidal glass, $k\xi_{\phi_g}^\psi$ should have a trivial value. Thus, m_ξ can be expressed as,

$$m_\xi = \psi k \xi_{\phi_g}^{\psi-1}\frac{d\xi}{d\phi/\phi_g}\Big|_{\phi=\phi_g} \sim \frac{d\ln\xi}{d\phi/\phi_g}\Big|_{\phi=\phi_g}. \tag{15}$$

We evaluated m_ξ using the last term in Eq (15) by extrapolating Eq (13) to $\xi_4 = \xi_{4,\phi_g}$. In Figure (6), we compare m_ξ with m_k, which shows that the two quantities are linearly related.

It is important to note that since the configurational entropy S_c decreases as $\phi \to \phi_K$ (or $T \to T_K$) [25, 84, 85], i.e., $S_c \sim \phi_K/\phi - 1$ (or $S_c \sim T/T_K - 1$), m_ξ can be written as a function of S_c,

$$m_\xi \sim \frac{dS_c^{-1}}{d\phi/\phi_g}\Big|_{\phi=\phi_g}, \tag{16}$$

which is consistent with the definition of the *thermodynamic fragility index* of liquids [86]. Therefore, the linear relation between m_ξ and m_k indicates that the thermodynamic and kinetic fragility indices of the charged colloids are proportional to one another. Such a proportionality has also been found for various types of molecular glasses. Martinez and Angell measured the kinetic and thermodynamic fragility index of various organic glasses and found that they had a linear relation for both strong and fragile glasses [86]. Similar behavior was also found by theories and simulations in polymeric glasses [87, 88], which implies that glass transition in soft colloids exhibits strong analogies to other molecular glasses. This also shows that the glass transition in simple and complex liquids manifest the universal features predicted by the RFOT theory.

CONCLUSIONS

We investigated the glass transition in binary charged charged colloids, which are excellent experimentally controllable model soft glasses, by performing extensive Brownian dynamics simulations. We showed that as concentration of monovalent salts is increased, the inter particle potential becomes soft. As a result, the characteristic glass transition volume fractions ϕ_d and ϕ_K decreases. In addition, we predict that by simply tuning the salt concentration, the fragility of the charged colloids varies greatly. The fragility value changes from about 10 at low salt concentration to in excess of 50 at high salt concentration values. Typically, the large values are associated with molecular systems that interact via anisotropic potentials. Surprisingly, in Wigner glasses, with isotropic inter particle interactions, the fragility varies continuously by altering a single from a low to high value by tuning a single externally controllable parameter.

Despite the changes in the softness of potential that is altered by addition of monovalent salts, the sluggish dynamics can be quantitatively described in terms of the enhanced dynamic heterogeneity as predicted by the RFOT theory. With the four-point dynamic structure factor as an appropriate order parameter, we determined the dynamic susceptibility and the associated increase in length scale by compressing the system. The simulations unambiguously show that the growth in the length scale with increasing ϕ is closely associated with the glassy dynamics, which is strikingly consistent with the prediction of the RFOT theory.

Using the RFOT theory, we found that the kinetic fragility index of the colloid can be expressed in terms of the length scales of the heterogeneous dynamics. This indicates that the kinetic and the thermodynamic fragility indices of the charged colloids should be linearly related as has been noted for both molecular glasses, such as organic and polymeric glasses. Thus, glass transition of diverse materials should be governed by the same universal principles, as anticipated by RFOT, regardless of a broad spectrum of their fragilities. The present simulations and recent developments show that RFOT provides a comprehensive theory of the structural glass transition by capturing quantitatively the onset of non-ergodicity, and divergence of a growing correlation length as the ideal transition density (or temperature) is approached from above. Because in Wigner glasses there is a smooth crossover from fragile to strong glass behavior, we can conclude that the single unified RFOT is sufficient to describe almost all aspects of glass forming materials.

ACKNOWLEDGEMENTS

This work was supported in part by a grant from National Science Foundation (CHE 19-00093) and the Collie-Welch Chair (F-0019) administered through the Welch Foundation.

Appendix A: Brownian Dynamics simulations

The position of the charged colloids is evolved using Brownian dynamics (BD) by numerically integrating the following equations of motion,

$$\frac{d\vec{r}_i}{dt} = \frac{D_{i,0}\vec{F}_i(t)}{k_B T}\delta t + \sqrt{2D_{i,0}}\vec{R}_i(t). \tag{17}$$

In Eq.17, δt is the integration time step, $\vec{r}_i(t)$ is the position vector of the i^{th} particle at time t, $\vec{F}_i(t)$ is the total systematic force acting on particle i, and $\vec{R}_i$ is the term for the fluctuation force that satisfies $\langle \vec{R}_i(t) \rangle = 0$ and $\langle \vec{R}_i(t) \cdot \vec{R}_i(t') \rangle = 6D_{i,0}\delta_{ij}\delta(t-t')$, where δ_{ij} and $\delta(t-t')$ are the Kronecker δ and the Dirac δ function, respectively. The diffusion coefficient, $D_{i,0}$, of the i^{th} particle in the infinitely dilute regime is chosen as 4.53 $\mu m^2/s$ and 2.24 $\mu m^2/s$ for the small and large colloids, respectively. Various values of the integration time step δt are considered for accuracy and efficiency of the simulation. We use $\delta t = 1$ μs for $\rho_r = 5$ and 10, $\delta t = 5$ μs for $\rho_r = 1$ and $\delta t = 10$ μs for $\rho_r = 0$, which provides numerical accuracy.

In order to generate equilibrium configurations, first we randomly placed the binary colloids in the cubic simulation box with periodic boundary conditions in all directions. The simulation box size L is determined by the value of ϕ, ranging from 4.1 μm to 67.9 μm. Then, we performed simulations for $t = 10\tau_\alpha \sim 100\tau_\alpha$ to obtain the equilibrium configuration, where τ_α is the structural relaxation time. After the equilibration step, we carried out additional BD simulations to calculate various dynamic properties of the system. We consider three independent trajectories for each set of ϕ and ρ_r to estimate ensemble averages of various properties. In the range of ϕ considered, reentrance behaviors of Wigner glasses were

not shown (see Appendix E). All the simulations were carried out with LAMMPS.

Appendix B: Comparison of structural relaxation time with viscosity

The self-part of the intermediate scattering function $F_q(t)$ characterizes the time-dependent density fluctuation on the length scale $l_q = 2\pi/q$. With appropriate choice of q, the relaxation time of $F_q(t)$ could capture the viscosity change of liquid near the glass transition [89]. Although the equivalence between τ_α and the shear viscosity η is often made, it is not always valid. Nevertheless, $F_q(t)$ is commonly estimated both in simulations and experiments to investigate the dynamics of the SGT.

Typically, two types of q are used,. One is q_{max} corresponding to the length scale l_{max} at the first maximum of the radial distribution function, and the second is q_{ave} related to the particle size. For liquids with steep potential such as hard spheres, q_{max} is comparable to q_{ave}, and is only marginally changed with a change in ϕ. Thus, the relaxation time τ_α obtained using the time-dependence of the $F_{q_{max}}(t)$ and $F_{q_{ave}}(t)$ does not result in qualitative difference in the characterizing relaxation dynamics in supercooled liquids. As shown in Figure 7 (A), however, for charged colloids, q_{max} varies significantly as ϕ increases although q_{ave} is invariant. This leads to a qualitatively different behavior of τ_α extracted from $F_{q_{max}}(t)$ and $F_{q_{ave}}(t)$ upon an increase in ϕ. When $\rho_r = 0$, for example, τ_α obtained from the decay of $F_{q_{ave}}(t)$ increases monotonically with ϕ, whereas that calculated from $F_{q_{max}}(t)$ has a minimum value (Figure 7 (B)). This implies that the description of glass transition of the charged colloids should depend on the value of q.

We confirm that τ_α extracted from the decay of $F_{q_{ave}}(t)$ is more relevant to the viscosity change as the system is compressed. We evaluate the shear viscosity η of the charged colloid using Green-Kubo formula,

$$\eta = \frac{V}{3k_BT}\int_0^\infty dt \sum_{(\alpha,\beta)'} \langle P_{\alpha,\beta}(t)P_{\alpha,\beta}(0)\rangle, \qquad (18)$$

where α and β denote Cartesian components (x, y and z), $(\alpha,\beta)'$ indicates the sum is over three different combinations of α and β. The pressure tensor $P_{\alpha,\beta}$ is defined as,

$$P_{\alpha,\beta} = \frac{1}{V}\sum_{i>j} \frac{r_{ij,\alpha}r_{ij,\beta}}{r_{ij}}\frac{\partial V(r_{ij})}{\partial r_{ij}}. \qquad (19)$$

In Eq (19), r_{ij} is the distance between particles i and j. The subscript α under the variable represents the α component in Cartesian coordinate. In Figure 7 (C), we plot τ_α versus η for various ρ_r. The colored filled circles show τ_α extracted from the time dependent behavior of$F_{q_{ave}}(t)$ as a function of η. The linear lines ($y \sim x$), used as a guide to the eyes, confirm the linearity between τ_α and η, indicating that τ_α from $F_{q_{ave}}(t)$ captures the

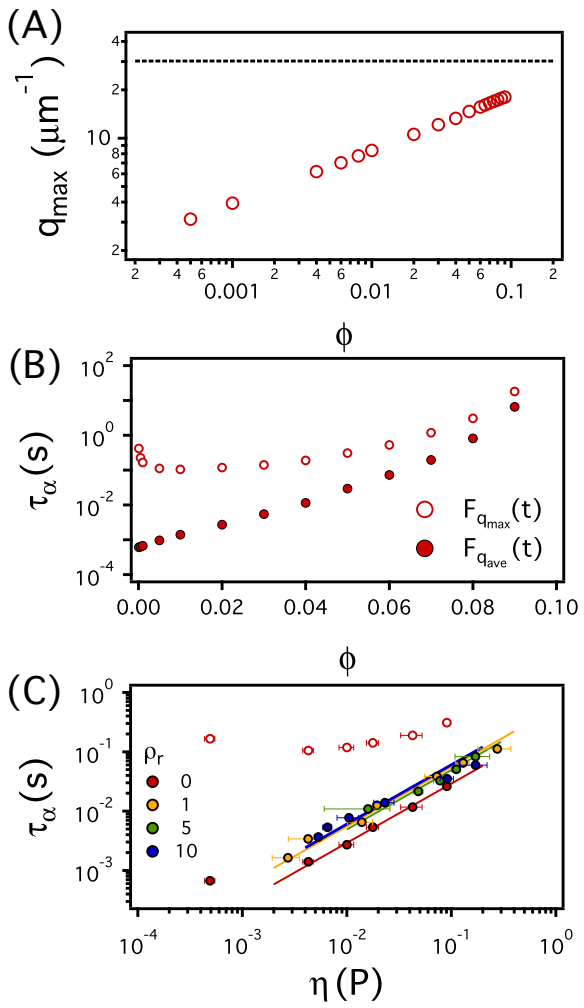

FIG. 7. (A) Dependence of q_{max} as a function of ϕ when $\rho_r = 0$ (the red circles); q_{max} is given by $2\pi/l_{max}$, where l_{max} is a length scale at which the radial distribution function has the first maximum. The black dashed line shows that $q_{ave} = 2\pi/d_{ave}$, where d_{ave} is the weight-averaged diameter of the charged colloidal particles, is independent of ϕ. (B) Comparison of τ_α obtained by $F_{q_{max}}(t)$ (the open red circles) and $F_{q_{ave}}(t)$ (the filled red circles) when $\rho_r = 0$. (C) Comparison of τ_α with η for various ρ_r. τ_α of the colored filled circles is obtained by $F_{q_{ave}}(t)$. The colored guide lines ($y \sim x$) confirm the linear relation of η with τ_α from $F_{q_{ave}}(t)$. The open red circles represent τ_α from $F_{q_{max}}(t)$ when $\rho_r = 0$, clearly indicating that $F_{q_{max}}(t)$ fails to capture the changes in η.

viscosity change of the charged colloidal particles accurately. On the other hand, the open red circles represent τ_α from $F_{q_{max}(t)}$ when $\rho_r = 0$, show that τ_α calculated from $F_{q_{max}}(t)$ and η do not correlate. Therefore, we use $F_{q_{ave}}(t)$ to characterize the glassy dynamics of the charged colloids.

Appendix C: Quantitative comparison of the DLVO potential with the hard sphere potential

Figure 1 (B) qualitatively shows that as ρ_r increases the DLVO potential approaches the hard sphere poten-

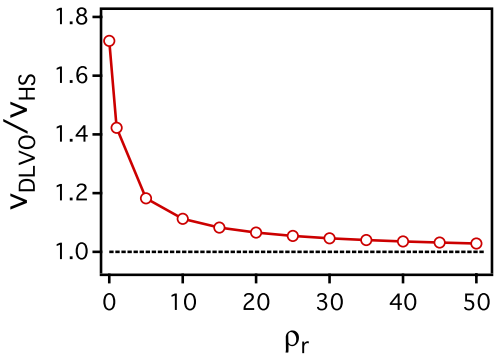

FIG. 8. Comparison of v_{DLVO} with v_{HS} as a function of ρ_r for larger charged colloids with $\phi = 0.4$.

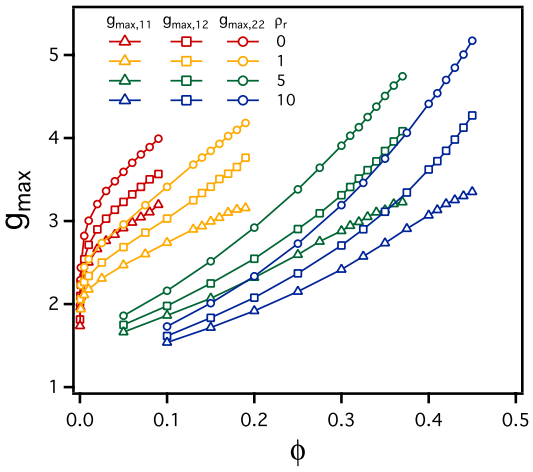

FIG. 9. $g_{max,11}$, $g_{max,12}$ and $g_{max,22}$ of the charged colloids as a function of ϕ at various ρ_r.

tial. In order to quantify the degree of the similarity between the DLVO potential with corresponding the hard sphere potential, we calculated their excluded volumes v_{DLVO} and v_{HS}, respectively, by relating it to the Mayer f-function, $v = 4\pi \int_0^\infty dr r^2(\exp[-V(r)/k_BT] - 1)$, where $V(r)$ is the interparticle potential. For hard spheres with diameter σ, $v_{HS} = (4\pi\sigma^3)/3$. However, for the DLVO potential with low ρ_r, v should exceed v_{HS}. In Figure 8, we plot v_{DLVO}/v_{HS} of the large charged colloids ($\sigma = 2.2\mu m$) as a function of ρ_r with $\phi = 0.4$. We find that v_{DLVO}/v_{HS} approaches 1 as ρ_r increases over 20. The difference between v_{DLVO} and v_{HS} is only less than 3% when $\rho_r = 50$, which means that the effective diameter ($\sim v^{1/3}$) differs by less than 1%. This suggests that for sufficiently large ρ_r, say $\rho_r = 50$, the charged colloids could be modeled by a hard sphere potential, implying that the glass transition behavior of Wigner glasses becomes hard-sphere like.

Appendix D: Hard sphere system as a reference for fragile glasses

To consider a reference system for fragile glasses, we perform a dynamic Monte Carlo simulation using binary hard sphere mixtures, which is found to reproduce well the dynamic light scattering (DLS) experiments of poly(methyl methacrylate) (PMMA) particles [67]. Diameters of the big and small hard spheres are $D_b = 1.4\sigma$ and $D_s = 1.0\sigma$, respectively, where σ is the reduced unit of length. We consider $N = 1000$ hard spheres (the numbers of big and small hard spheres are equal). The positions of the hard spheres are evolved using dynamic Monte Carlo (dMC) simulation with a standard Metropolis algorithm. At every Monte Carlo step, a particle is randomly chosen and displaced by a random vector, whose components for each direction are randomly drawn between -0.1σ and 0.1σ. The unit time t is defined as the number of MC steps divided by N. Initial configuration is prepared by randomly placing the non-overlapped hard spheres in a periodically replicated (in all dimensions) three dimensional simulation box. We equilibrated the initial configurations by performing dMC simulations for $t = 10\tau_\alpha \sim 100\tau_\alpha$, then production run was performed to obtain the relaxation time τ_α which is determined as a characteristic time scale in the decay of $F_q(t)$ with $q\sigma = 6.1$. We considered ϕ from 0.5 to 0.59. For each volume fraction ϕ, three to five ensembles are used to perform an ensemble average.

Appendix E: Peak values of the radial distribution function as a function of ϕ

For hard sphere colloids, the height of the peak of the static structure factor $S(q)$ or that of the radial distribution function $g(r)$ increases monotonically with an increase in ϕ. For the soft colloids, however, they first increase with ϕ but begin to decrease at a certain volume fraction [90, 91]. This is attributed to non-equilibrium dynamic behavior due to aging or a compressed exponential decay of $F_q(t)$ [37, 52].

In the range of ϕ considered in this work, we did not such non-equilibrium effects. We consider three radial distribution functions $g_{11}(r)$, $g_{12}(r)$, and $g_{22}(r)$ of the charged colloids, where $g_{i,j}(r)$ is the radial distribution function between i and j types of colloids, and the values 1 and 2 indicate small and large colloids, respectively. Figure 9 plots their peak values $g_{max,11}$, $g_{max,12}$, and $g_{max,22}$ as a function of ϕ at various ρ_r, indicating that all of them increase monotonously in the range of ϕ considered in this study. This behavior, reminiscent of hard spheres, shows that standard feature of charged colloids may be mapped onto an equivalent hard sphere system with a much larger effective diameter [68].

Appendix F: Individual fits to data in Figure 5 (C)

In order to investigate finite size effects on the value of ϕ_K for a given ρ_r, we first evaluated τ_α of various ϕ with N. Note that the simulation box size L is varied with ϕ as, $L = \left(\frac{4}{3}\pi\frac{a_1^3+a_2^3}{\phi}\right)^{1/3}$ since N is fixed. Then, we estimated $\phi_{K,N}$ with a VFT fit (Eq (4)). We repeated

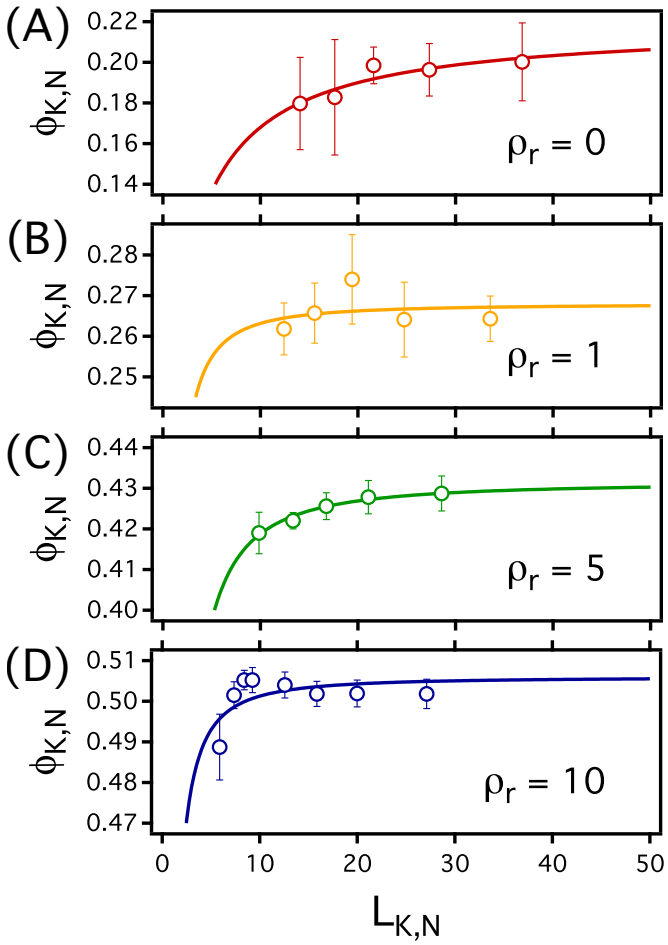

FIG. 10. Individual fits of Figure 5 (C). $\phi_{K,N}$ is ϕ_K at N, which is obtained by the VFT fit as in Figure 2 (C). In the each panel, $\phi_{K,N}$ of $L_{K,N}$ (the open circles) is fitted to Eq (12) (the solid lines), by which $\phi_{K,\infty}$ and L_0 are obtained as fitting parameters.

this process to obtain $\phi_{K,N}$ for various N, and compared $\phi_{K,N}$ of $L_{K,N}$ with Eq (12). N ranges from $N = 500$ to $N = 10,000$ for $\rho_r = 0$ and from $N = 100$ to $N = 10000$ for $\rho_r = 1, 5$, and 10.

In Figure 10, we show how $\phi_{K,N}$ changes with $L_{K,N}$ as a function of N. The value of $L_{K,N}$ is given by $(N.\phi_{K,N})^{1/3}$. The ρ_r values are shown in Figure 10.

[1] T. R. Kirkpatrick, D. Thirumalai, and P. G. Wolynes, "*Scaling Concepts for the Dynamics of Viscous Liquids near an Ideal Glassy State*," Phys. Rev. A **40**, 1045–1054 (1989).

[2] T. R. Kirkpatrick and D. Thirumalai, "*Are Disordered Spin Glass Models Relevant for the Structural Glass Problem?*" Transp. Theor. Stat. Phys. **24**, 927 (1995).

[3] V. Lubchenko and P. G. Wolynes, "*Theory of Structural Glasses and Supercooled Liquids*," Ann. Rev. Phys. Chem. **58**, 235–266 (2007).

[4] G. Parisi and F. Zamponi, "*Mean-Field Theory of Hard Sphere Glasses and Jamming*," Rev. Mod. Phys. **82**, 789–845 (2010).

[5] L. Berthier and G. Biroli, "*Theoretical Perspective on the Glass Transition and Amorphous Materials*," Rev. Mod. Phys. **83**, 587–645 (2011).

[6] G. Biroli and J. P. Bouchaud, "*The Random First-Order Transition Theory of Glasses: A Critical Assessment*," in *Structural Glasses and Supercooled Liquids* (John Wiley & Sons, New York, 2012) Chap. 2, pp. 31–113.

[7] T. R. Kirkpatrick and D. Thirumalai, "*Colloquium: Random First Order Transition Theory Concepts in Biology and Physics*," Rev. Mod. Phys. **87**, 183–209 (2015).

[8] T. R. Kirkpatrick and D. Thirumalai, "*Dynamics of the Structural Glass Transition and the p-Spin—Interaction Spin-Glass Model*," Phys. Rev. Lett. **58**, 2091–2094 (1987).

[9] T. R. Kirkpatrick and D. Thirumalai, "*P-Spin-Interaction Spin-Glass Models: Connections with the Structural Glass Problem*," Phys. Rev. B **36**, 5388–5397 (1987).

[10] T. R. Kirkpatrick and P. G. Wolynes, "*Stable and Metastable States in Mean-Field Potts and Structural Glasses*," Phys. Rev. B **36**, 8552–8564 (1987).

[11] T. R. Kirkpatrick and D. Thirumalai, "*Mean-Field Soft-Spin Potts Glass Model: Statics and Dynamics*," Phys. Rev. B **37**, 5342–5350 (1988).

[12] D. Thirumalai and T. R. Kirkpatrick, "*Mean-field Potts Glass Model: Initial-Condition Effects on Dynamics and Properties of Metastable States*," Phys. Rev. B **38**, 4881–4892 (1988).

[13] T. R. Kirkpatrick and D. Thirumalai, "Random solutions from a regular density functional hamiltonian: a static and dynamical theory for the structural glass transition," J. Phys. A **22**, L149–L155 (1989).

[14] JP Bouchaud and M Mezard, "Self-Induced Quenched Disorder - A Model for the Glass Transition," J. de Physique I **4**, 1109–1114 (1994).

[15] S Franz and J Hertz, "Glassy Transition and Aging in a Model Without Disorder," Phys. Rev. Lett. **74**, 2114–2117 (1995).

[16] T. R. Kirkpatrick and P. G. Wolynes, "Connections between some kinetic and equilibrium theories of the glass transition," Phys. Rev. A **35**, 3072–3080 (1987).

[17] J. Kurchan, G. Parisi, and F. Zamponi, "*Exact Theory of Dense Amorphous Hard Spheres in High Dimension. I. The Free Energy*," J. Stat. Mech. **2012**, P10012 (2012).

[18] J. Kurchan, G. Parisi, P. Urbani, and F. Zamponi, "*Exact Theory of Dense Amorphous Hard Spheres in High Dimension. II. The High Density Regime and the Gardner Transition*," J. Phys. Chem. B **117**, 12979–12994 (2013).

[19] P. Charbonneau, J. Kurchan, G. Parisi, P. Urbani, and F. Zamponi, "*Exact theory of dense amorphous hard spheres in high dimension. III. The full replica symmetry breaking solution*," J. Stat. Mech. **2014**, P10009 (2014).

[20] H M Lindsay and P M Chaikin, "*Elastic Properties of Colloidal Crystals and Glasses*," J. Chem. Phys. **76**, 3774–3781 (1982).

[21] D Thirumalai and RD Mountain, "Activated dynamics, loss of ergodicity, and transport in supercooled liquids," hys. Rev. E. **47**, 479–489 (1993).

[22] RD Mountain and D Thirumalai, "Molecular-dynamics

study of glassy and supercooled states of a binary mixture of soft spheres," Phys. Rev. A **36**, 3300–3311 (1987).

[23] W. Kob, S. Roldán-Vargas, and L. Berthier, "*Non-Monotonic Temperature Evolution of Dynamic Correlations in Glass-Forming Liquids*," Nat. Phys. **8**, 164–167 (2011).

[24] M. Ozawa, W. Kob, A. Ikeda, and K. Miyazaki, "*Equilibrium Phase Diagram of a Randomly Pinned Glass-Former*," Proc. Natl. Acad. Sci. U. S. A. **112**, 6914–6919 (2015).

[25] L. Berthier, P. Charbonneau, D. Coslovich, A. Ninarello, M. Ozawa, and S. Yaida, "*Configurational Entropy Measurements in Extremely Supercooled Liquids that Break the Glass Ceiling*," Proc. Natl. Acad. Sci. U. S. A. **114**, 11356–11361 (2017).

[26] G Biroli, J-P Bouchaud, A Cavagna, T S Grigera, and P Verrocchio, "*Thermodynamic signature of growing amorphous order in glass-forming liquids*," Nat. Phys. **4**, 771–775 (2008).

[27] L. Berthier and R. L. Jack, "*Evidence for a Disordered Critical Point in a Glass-Forming Liquid*," Phys. Rev. Lett. **114**, 205701 (2015).

[28] K. Hima Nagamanasa, S. Gokhale, A. K. Sood, and R. Ganapathy, "*Direct Measurements of Growing Amorphous Order and Non-Monotonic Dynamic Correlations in a Colloidal Glass-Former*," Nat. Phys. **11**, 403–408 (2015).

[29] D. Ganapathi, K. Hima Nagamanasa, A. K. Sood, and R. Ganapathy, "*Measurements of Growing Surface Tension of Amorphous–Amorphous Interfaces on Approaching the Colloidal Glass Transition*," Nat. Commun. **9**, 397 (2018).

[30] S. Gokhale, A. K. Sood, and R. Ganapathy, "*Deconstructing the Glass Transition through Critical Experiments on Colloids*," Adv. Phys. **65**, 363–452 (2016).

[31] S. Albert, T. Bauer, M. Michl, G. Biroli, J. P. Bouchaud, A. Loidl, P. Lunkenheimer, R. Tourbot, C. Wiertel-Gasquet, and F. Ladieu, "*Fifth-Order Susceptibility Unveils Growth of Thermodynamic Amorphous Order in Glass-Formers*," Science **352**, 1308–1311 (2016).

[32] C. A. Angell, "*Formation of Glasses from Liquids and Biopolymers*," Science **267**, 1924–1935 (1995).

[33] R. Böhmer, K. L. Ngai, C. A. Angell, and D. J. Plazek, "*Nonexponential Relaxations in Strong and Fragile Glass Formers*," J. Chem. Phys. **99**, 4201–4209 (1993).

[34] P. C. Royall, W. C. K. Poon, and E. R. Weeks, "*In Search of Colloidal Hard Spheres*," Soft Matter **9**, 17–27 (2013).

[35] J. Mattsson, H. M. Wyss, A. Fernandez-Nieves, K. Miyazaki, Z. Hu, D. R. Reichman, and D. A. Weitz, "*Soft Colloids Make Strong Glasses*," Nature **462**, 83–86 (2009).

[36] P. van der Scheer, T. van de Laar, J. van der Gucht, D. Vlassopoulos, and J. Sprakel, "*Fragility and Strength in Nanoparticle Glasses*," ACS Nano **11**, 6755–6763 (2017).

[37] A. M. Philippe, D. Truzzolillo, J. Galvan-Myoshi, P. Dieudonné-George, V. Trappe, L. Berthier, and L. Cipelletti, "*Glass Transition of Soft Colloids*," Phys. Rev. E **97**, 040601 (2018).

[38] Abdul N. Malmi-Kakkada, Xin Li, Himadri S. Samanta, Sumit Sinha, and D. Thirumalai, "*Cell Growth Rate Dictates the Onset of Glass to Fluidlike Transition and Long Time Superdiffusion in an Evolving Cell Colony*," Phys. Rev. X **8**, 021025 (2018).

[39] T. E. Angelini, E. Hannezo, X. Trepat, M. Marquez, J. J. Fredberg, and D. A. Weitz, "*Glass-Like Dynamics of Collective Cell Migration*," Proceedings of the National Academy of Sciences **108**, 4714–4719 (2011).

[40] R. P. Seekell III, P. S. Sarangapani, Z. Zhang, and Y. Zhu, "*Relationship between Particle Elasticity, Glass Fragility, and Structural Relaxation in Dense Microgel Suspensions*," Soft Matter **11**, 5485–5491 (2015).

[41] V. Nigro, B. Ruzicka, B. Ruta, F. Zontone, M. Bertoldo, E. Buratti, and R. Angelini, "*Structural relaxation, softness and fragility of IPN Microgels*," arXiv:1807.01692v2 [cond-mat.soft] (2018).

[42] V. Nigro, R. Angelini, M. Bertoldo, F. Bruni, M. A. Ricci, and B. Ruzicka, "*Dynamical Behavior of Microgels of Interpenetrated Polymer Networks*," Soft Matter **13**, 5185–5193 (2017).

[43] J. Yang and K. S. Schweizer, "*Tunable Dynamic Fragility and Elasticity in Dense Suspensions of Many-Arm-Star Polymer Colloids*," Europhys. Lett. **90**, 66001 (2010).

[44] C. A. Angell and K. Ueno, "*Materials Science: Soft Is Strong*," Nature **462**, 45–46 (2009).

[45] D. Saha, Y. M. Joshi, and R. Bandyopadhyay, "*Kinetics of the Glass Transition of Fragile Soft Colloidal Suspensions*," J. Chem. Phys. **143**, 214901 (2015).

[46] Q. Li, X. Peng, and G. B. McKenna, "*Long-term Aging Behaviors in a Model Soft Colloidal System*," Soft Matter **13**, 1396–1404 (2017).

[47] A. Ninarello, L. Berthier, and D. Coslovich, "*Models and Algorithms for the Next Generation of Glass Transition Studies*," Phys. Rev. X **7**, 021039 (2017).

[48] Z. Shi, P. G. Debenedetti, F. H. Stillinger, and P. Ginart, "*Structure, Dynamics, and Thermodynamics of a Family of Potentials with Tunable Softness.*" J. Chem. Phys. **135**, 084513 (2011).

[49] C. D. Michele, F. Sciortino, and A. Coniglio, "*Scaling in Soft Spheres: Fragility Invariance on the Repulsive Potential Softness*," J. Phys.: Condens. Matt. **16**, L489–L494 (2004).

[50] Johannes Krausser, Konrad H. Samwer, and Alessio Zaccone, "Interatomic repulsion softness directly controls the fragility of supercooled metallic melts," Proc. Natl. Acad. Sci. **112**, 13762–13767 (2015).

[51] M. Asai, A. Cacciuto, and S. K. Kumar, "*Surface Fluctuations Dominate the Slow Glassy Dynamics of Polymer-Grafted Colloid Assemblies*," ACS Cent. Sci. **4**, 1179–1184 (2018).

[52] N. Gnan and E. Zaccarelli, "*The Microscopic Role of Deformation in the Dynamics of Soft Colloids*," Nat. Phys. **15**, 683–688 (2019).

[53] T. R. Kirkpatrick and D. Thirumalai, "Universal Aspects of the Random First Order Phase Transition Theory of the Structural Glass Transition," arXiv:1401.2024 [cond-mat.stat-mech] (2014).

[54] J. P. Bouchaud and G. Biroli, "*On the Adam-Gibbs-Kirkpatrick-Thirumalai-Wolynes Scenario for the Viscosity Increase in Glasses*," J. Chem. Phys. **121**, 7347–7354 (2004).

[55] L. Berthier and W. Kob, "*Static Point-to-Set Correlations in Glass-Forming Liquids*," Phys. Rev. E **85**, 011102 (2012).

[56] E. Flenner and G. Szamel, "*Fundamental Differences between Glassy Dynamics in Two and Three Dimensions*," Nat. Commun. **6**, 7392 (2015).

[57] E. Flenner, M. Zhang, and G. Szamel, "*Analysis of a Growing Dynamic Length Scale in a Glass-Forming Binary Hard-Sphere Mixture*," Phys. Rev. E **83**, 051501 (2011).

[58] E. Flenner, H. Staley, and G. Szamel, "*Universal Features of Dynamic Heterogeneity in Supercooled Liquids*," Phys. Rev. Lett. **112**, 097801 (2014).

[59] E. Flenner and G. Szamel, "*Dynamic Heterogeneity in a Glass Forming fluid: Susceptibility, Structure Factor, and Correlation Length*," Phys. Rev. Lett. **105**, 217801 (2010).

[60] R. O. Rosenberg, D. Thirumalai, and R. D. Mountain, "*Liquid, Crystalline and Glassy States of Binary Charged Colloidal Suspensions*," J. Phys. Condens. Mat. **1**, 2109–2114 (1989).

[61] H. Kang, T. R. Kirkpatrick, and D. Thirumalai, "*Manifestation of Random First-Order Transition Theory in Wigner Glasses*," Phys. Rev. E **88**, 042308 (2013).

[62] S. Alexander, P. M. Chaikin, P. Grant, G. J. Morales, P. Pincus, and D. Hone, "*Charge Renormalization, Osmotic Pressure, and Bulk Modulus of Colloidal Crystals: Theory*," J. Chem. Phys. **80**, 5776–5781 (1984).

[63] R. O. Rosenberg and D. Thirumalai, "*Order-Disorder Transition in Colloidal Suspensions*," Phys. Rev. A **36**, 5690–5700 (1987).

[64] S. Sanyal and A. K Sood, "*Brownian Dynamics Simulation of Dense Binary Colloidal Mixtures. I. Structural Evolution and Dynamics*," Phys. Rev. E **52**, 4154–4167 (1995).

[65] D. Thirumalai, "*Liquid and Crystalline States of Monodisperse Charged Colloidal Particles*," J. Phys. Chem. **93**, 5637–5644 (1989).

[66] M. E. Fisher, Y. Levin, and X. Li, "*The Interaction of Ions in an Ionic Medium*," J. Chem. Phys. **101**, 2273–2282 (1994).

[67] G. Brambilla, D. El Masri, M. Pierno, L. Berthier, L. Cipelletti, G. Petekidis, and A. B. Schofield, "Probing the Equilibrium Dynamics of Colloidal Hard Spheres above the Mode-Coupling Glass Transition," Phys. Rev. Lett. **102**, 085703 (2009).

[68] RO Rosenberg and D Thirumalai, "Structure and Dynamics of Screened-Coulomb Colloidal Liquids," Phys. Rev. A **33**, 4473–4476 (1986).

[69] A. Ikeda, L. Berthier, and P. Sollich, "*Disentangling Glass and Jamming Physics in the Rheology of Soft Materials*," Soft Matter **9**, 7669–7683 (2013).

[70] K. Chen, W. G. Ellenbroek, Z. Zhang, D. T. N. Chen, P. J. Yunker, S. Henkes, C. Brito, O. Dauchot, W. van Saarloos, A. J. Liu, and A. G. Yodh, "*Low-Frequency Vibrations of Soft Colloidal Glasses*," Phys. Rev. Lett. **105**, 025501 (2010).

[71] D. Thirumalai, Raymond D. Mountain, and T. R. Kirkpatrick, "*Ergodic Behavior in Supercooled Liquids and in Glasses*," Phys. Rev. A **39**, 3563–3574 (1989).

[72] G. Biroli and J. P Garrahan, "*Perspective: The Glass Transition*," J. Chem. Phys. **138**, 12A301 (2013).

[73] M. D. Ediger, "*Spatially Heterogeneous Dynamics in Supercooled Liquids*," Ann. Rev. Phys. Chem. **51**, 99–128 (2000).

[74] M. D. Ediger and P. Harrowell, "*Perspective: Supercooled Liquids and Glasses*," J. Chem. Phys. **137**, 080901 (2012).

[75] T. R. Kirkpatrick and D. Thirumalai, "*Comparison between Dynamical Theories and Metastable States in Regular and Glassy Mean-Field Spin Models with Underlying First-Order-Like Phase Transitions*," Phys. Rev. A **37**, 4439–4448 (1988).

[76] N. Lačević, F. W. Starr, T. B. Schrøder, and S. C. Glotzer, "*Spatially Heterogeneous Dynamics Investigated via a Time-Dependent Four-Point Density Correlation Function*," J. Chem. Phys. **119**, 7372–7387 (2003).

[77] S. Karmakar, C. Dasgupta, and S. Sastry, "*Analysis of Dynamic Heterogeneity in a Glass Former from the Spatial Correlations of Mobility.*" Phys. Rev. Lett. **105**, 015701 (2010).

[78] E. Flenner and G. Szamel, "Characterizing Dynamic Length Scales in Glass-Forming Liquids," Nat. Phys. **8**, 696–697 (2012).

[79] C. Cammarota, A. Cavagna, I. Giardina, G. Gradenigo, T. S. Grigera, G. Parisi, and P. Verrocchio, "*Phase-Separation Perspective on Dynamic Heterogeneities in Glass-Forming Liquids*," Phys. Rev. Lett. **105**, 055703 (2010).

[80] M. Ozawa, C. Scalliet, A. Ninarello, and L. Berthier, "*Does the Adam-Gibbs Relation Hold in Simulated Supercooled Liquids?*" arXiv:1905.08179v1 [cond-mat.stat-mech] (2019).

[81] J. D. Stevenson, J. Schmalian, and P. G. Wolynes, "*The Shapes of Cooperatively Rearranging Regions in Glass-Forming Liquids*," Nat. Phys. **2**, 268–274 (2006).

[82] L. Berthier, G. Biroli, J. P. Bouchaud, and R. L. Jack, "*Overview of Different Characterizations of Dynamic Heterogeneity*," in *Dynamical Heterogeneities in Glasses, Colloids, and Granular Media* (Oxford University Press, 2011) Chap. 3.

[83] T. Bauer, P. Lunkenheimer, and A. Loidl, "*Cooperativity and the Freezing of Molecular Motion at the Glass Transition*," Phys. Rev. Lett. **111**, 225702 (2013).

[84] M. Ozawa, G. Parisi, and L. Berthier, "*Configurational Entropy of Polydisperse Supercooled Liquids*," J. Chem. Phys. **149**, 154501 (2018).

[85] L. Berthier, M. Ozawa, and C. Scalliet, "*Configurational Entropy of Glass-Forming Liquids*," J. Chem. Phys. **150**, 160902 (2019).

[86] L. M. Martinez and C. A. Angell, "*A Thermodynamic Connection to the Fragility of Glass-Forming Liquids*," Nature **410**, 663–667 (2001).

[87] J. Dudowicz, K. F Freed, and J. F Douglas, "*Fragility of Glass-Forming Polymer Liquids*," J. Phys. Chem. B **109**, 21350–21356 (2005).

[88] F. W. Starr and J. F. Douglas, "*Modifying Fragility and Collective Motion in Polymer Melts with Nanoparticles*," Phys. Rev. Lett. **106**, 115702 (2011).

[89] S. Sengupta, S. Karmakar, C. Dasgupta, and S. Sastry, "*Breakdown of the Stokes-Einstein Relation in Two, Three, and Four Dimensions*," J. Chem. Phys. **138**, 12A548 (2013).

[90] Z. Zhang, N. Xu, D. T. N. C., P. Yunker, A. M. Alsayed, K. B. Aptowicz, P. Habdas, A. J. Liu, S. R. Nagel, and A. G. Yodh, "*Thermal Vestige of the Zero-Temperature Jamming Transition*," Nature **459**, 230–233 (2009).

[91] D. Paloli, P. S. Mohanty, J. J. Crassous, E. Zaccarelli, and P. Schurtenberger, "Fluid-solid transitions in soft-repulsive colloids," Soft Matter **9**, 3000–3004 (2013).